

PhysDrape: Learning Explicit Forces and Collision Constraints for Physically Realistic Garment Draping

Minghai Chen^{1,2}, Mingyuan Liu^{1,3}, and Yuxiang Huan¹

¹ Guangdong Institute of Intelligence Science and Technology, China

² Macau University of Science and Technology, Macau SAR, China

³ Beihang University, China

{chenminghai, liumingyuan, huanyuxiang}@gdiist.cn

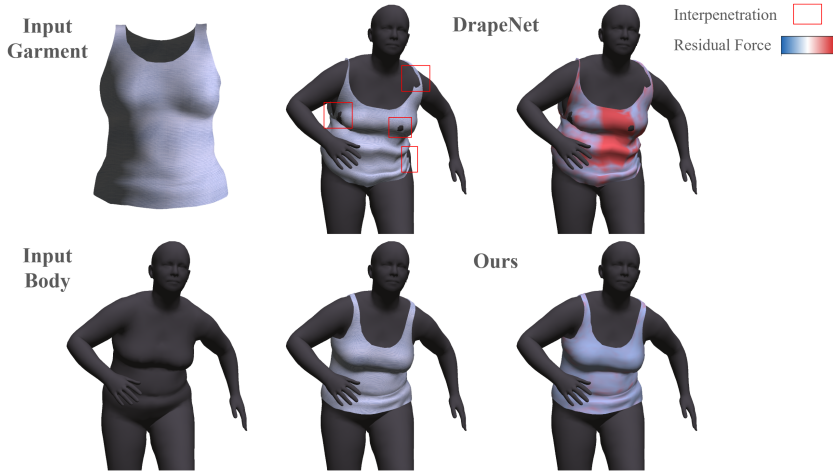


Fig. 1: Our method effectively resolves complex collisions and dissipates residual force, generating geometrically consistent and physically relaxed garments, whereas the baseline suffers from severe interpenetration (highlighted in red boxes) and high residual force (red regions in the force heatmap).

Abstract. Deep learning-based garment draping has emerged as a promising alternative to traditional Physics-Based Simulation (PBS), yet robust collision handling remains a critical bottleneck. Most existing methods enforce physical validity through soft penalties, creating an intrinsic trade-off between geometric feasibility and physical plausibility: penalizing collisions often distorts mesh structure, while preserving shape leads to interpenetration. To resolve this conflict, we present PhysDrape, a hybrid neural-physical solver for physically realistic garment draping driven by explicit forces and constraints. Unlike soft-constrained frameworks, PhysDrape integrates neural inference with explicit geometric solvers in a fully differentiable pipeline. Specifically, we propose a Physics-Informed Graph Neural Network conditioned on a physics-enriched graph—encoding material parameters and body proximity—to

predict residual displacements. Crucially, we integrate a differentiable two-stage solver: first, a learnable Force Solver iteratively resolves unbalanced forces derived from the Saint Venant-Kirchhoff (StVK) model to ensure quasi-static equilibrium; second, a Differentiable Projection strictly enforces collision constraints against the body surface. This differentiable design guarantees physical validity through explicit constraints, while enabling end-to-end learning to optimize the network for physically consistent predictions. Extensive experiments demonstrate that Phys-Drape achieves state-of-the-art performance, ensuring negligible interpenetration with significantly lower strain energy compared to existing baselines, achieving superior physical fidelity and robustness in real-time.

Keywords: Neural Garment Simulation · Collision Handling · Graph Neural Networks

1 Introduction

Automatic garment draping is fundamental to a wide range of applications, including virtual try-on, animation, video gaming, and the emerging metaverse [16, 41, 49]. While traditional Physics-Based Simulation (PBS) [1, 10, 24, 29–31, 35, 36, 43, 47, 50] guarantees high physical fidelity and collision-free results, it relies on expensive solvers that are computationally intensive, limiting its application in large-scale real-time applications.

To overcome these computational bottlenecks, recent years have witnessed the emergence of learning-based approaches aiming to approximate the draping process with real-time inference speeds while maintaining differentiability. Early methods [4, 5, 13, 14, 33, 38] often relied on supervised learning, training neural networks to regress garment geometry from body poses. However, these approaches face significant scalability challenges: they require massive ground-truth datasets obtained from computationally expensive simulations or complex 3D scanning setups. Furthermore, to handle unseen garments or extreme poses, such methods would require collecting an impractical amount of data to cover diverse garment-body combinations.

In response to these challenges, physics-based self-supervision has emerged as a promising direction, constraining predictions to obey physical laws without requiring ground-truth data. Pioneering works [3, 39] introduced optimization frameworks tailored for specific garments, while subsequent methods [9, 12, 19, 22, 46] extended this capability to generalize across diverse garment topologies. Despite their success, a fundamental limitation persists across these neural solvers: they predominantly enforce physical validity through soft penalty terms in the loss function. This formulation induces an intrinsic trade-off: aggressively penalizing collisions often leads to geometric distortion and non-physical stretching, whereas prioritizing structural preservation inevitably permits interpenetration. Consequently, soft-constrained formulations struggle to guarantee both strict collision constraint and physical fidelity simultaneously. While learned correctors [44, 45] attempt to address this via predictive offsets, they rely on ground-truth supervision and lack explicit solvers to ensure physical equilibrium.

In this work, we present PhysDrape, a hybrid neural-physical solver designed to bridge the gap between neural efficiency and explicit physical constraints. Unlike frameworks that implicitly trade off geometric feasibility against physical plausibility, PhysDrape tightly couples a Graph Neural Network (GNN) with a learnable explicit solver. By integrating a fully differentiable projection layer, we unify prediction and correction into an end-to-end learning framework, where collision constraints serve as differentiable supervision to enforce physically plausible results.

To summarize, our main contributions are:

- We propose PhysDrape, a hybrid framework that resolves the conflict between collision handling and structural preservation by integrating neural inference with explicit geometric solvers in a differentiable loop.
- We design a Physics-Informed GNN to predict candidate deformations, which are refined by a two-stage solver: a learnable Force Solver that minimizes Saint Venant-Kirchhoff (StVK) residual forces, and a differentiable projection layer that strictly enforces collision constraints.
- We demonstrate that PhysDrape achieves state-of-the-art performance. Our method ensures negligible interpenetration with significantly lower strain energy compared to baselines, while maintaining real-time inference speeds.

2 Related Works

2.1 Modeling 3D Garment Draping

Approaches for garment draping generally fall into two categories: explicit physical simulation and learning-based approximations. Explicit Physical Simulation models cloth dynamics using Mass-Spring Systems (MSS) [36] or Finite Element Methods (FEM) [11], typically employing optimization-based solvers like Position-Based Dynamics (PBD) [28], Extended PBD (XPBD) [26], and Projective Dynamics (PD) [6] for stability. However, integrating these solvers into deep learning frameworks faces severe bottlenecks. Standard explicit schemes rely on non-differentiable discrete projections, while differentiable variants like DiffXPBD [42] and rigorous collision solvers like IPC [18] necessitate adjoint-based backward passes or global Hessian construction. These operations require solving large linear systems at every step, causing gradient instability (e.g., exploding/vanishing) and prohibiting real-time inference.

Learning-based approaches have emerged as efficient alternatives to overcome the computational bottlenecks and limitations of traditional solvers. Early methods [4, 5, 13, 14, 33, 38] adopted supervised paradigms, training neural networks to regress garment geometry from body poses. These methods suffer from poor scalability due to their heavy reliance on massive ground-truth datasets obtained from expensive offline simulations. To eliminate the reliance on expensive generated data, SNUG [39] and PBNS [3] pioneered physics-based self-supervision, training networks by minimizing physical energies directly. Santesteban et al. [40] proposed a generative framework that utilizes a diffused body representation to

explicitly target collision handling. GAPS [7] introduced a collision-aware geometrical loss to enforce inextensibility, allowing adaptive stretching to resolve interpenetrations.

However, these approaches are typically confined to specific garment templates, limiting their applicability to unseen topologies. To address this, DIG [20] pioneered the use of implicit Signed Distance Functions (SDF) [32] for draping. By learning a continuous skinning field, DIG handles arbitrary garment geometries and reconstructs meshes via the Marching Cubes algorithm [17]. Despite its topological flexibility, DIG relies on fully supervised training with ground-truth meshes and is restricted to watertight geometries, failing to handle open surfaces. Building on this, DrapeNet [9] eliminates the reliance on supervision by integrating physics-based objectives into a generative framework based on Unsigned Distance Functions (UDF) [8, 48, 52]. This formulation enables the realistic draping of open, non-watertight surfaces in a fully self-supervised manner. Further advancing this direction, ISP [19] introduces implicit sewing patterns to model complex multi-layered garments. Despite their topological flexibility, these implicit-based methods fundamentally rely on soft penalties, inducing an unavoidable trade-off between preventing interpenetrations and preserving structural fidelity, limiting their utility in rigorous physical applications.

2.2 Collision Handling in Neural Draping

Resolving garment-body interpenetration remains a critical bottleneck in neural garment simulation. Early approaches often relied on geometric post-processing [38] to project penetrating vertices onto the body surface, but this naive projection ignores physical constraints, yielding non-physical distortions. To enable end-to-end learning, most neural solvers [3, 9, 39] rely on soft collision penalties. Recently, SENC [22] extended this paradigm to handle self-collisions via a global intersection volume loss. Fundamentally, these approaches induce a intrinsic trade-off between geometric validity and structural fidelity. Learned corrector modules have been proposed to address this; ReFU [44] introduces a learnable unit to predict displacement scales for SDF-based repulsion, while SAF [45] extends this correction to the face domain using local triangle features. However, treating collision handling as a regression task relies on generalization rather than strict constraint satisfaction. These methods lack explicit constraints to enforce non-penetration on unseen poses or dissipate residual energy, leading to unresolved force imbalances. In contrast, PhysDrape integrates a deterministic projection solver directly into the end-to-end learning pipeline. This design enables the network to coordinate with strict geometric constraints to achieve negligible interpenetration, while learning to minimize total potential energy. Simultaneously, an explicit force solver actively dissipates residual forces, ensuring physical fidelity in a fully self-supervised manner.

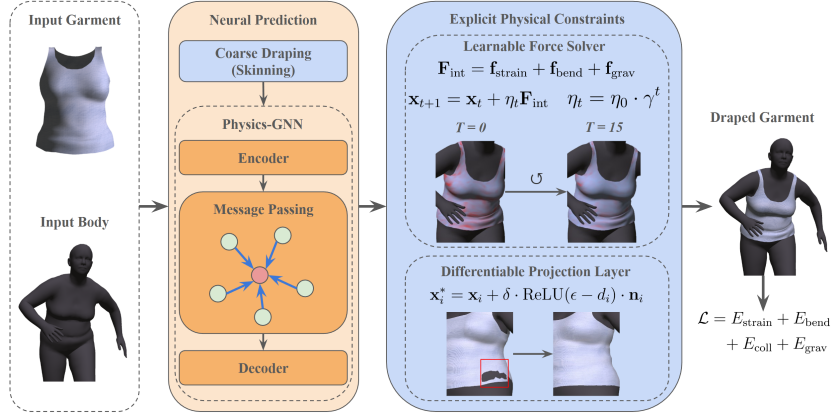


Fig. 2: Overview of PhysDrape. The pipeline begins with a coarse initialization generated via Linear Blend Skinning on the SMPL body. A Physics-Informed GNN then predicts residual displacements to recover geometric details. To guarantee physical validity, the prediction is refined by a two-stage differentiable module: a Learnable Force Solver that iteratively resolves unbalanced forces from StVK deformation, and a Differentiable Projection Layer that strictly enforces collision constraints.

3 Methods

3.1 Overview

Fig. 2 illustrates the overall pipeline of PhysDrape. We aim to predict the quasi-static equilibrium of garments, guaranteeing both physical fidelity and collision avoidance. We use the Saint Venant-Kirchhoff (StVK) material to model garments with varying stiffness parameters. To this end, we propose a hybrid framework that couples a Physics-Informed GNN with explicit differentiable solvers. The pipeline begins by generating a coarse, pose-dependent initialization $\mathbf{X}_{\text{coarse}}$ fitting the SMPL body [25]:

$$\begin{aligned} \mathbf{X}_{\text{coarse}} &= W(\mathbf{X}_{\text{shape}}, \beta, \theta, \mathcal{W}_G), \\ \mathbf{X}_{\text{shape}} &= \mathbf{V}_{\text{temp}} + \Delta \mathbf{X}_{\text{shape}}(\mathbf{V}_{\text{temp}}, \beta), \end{aligned} \quad (1)$$

where \mathbf{V}_{temp} denotes template vertices, and θ represents body pose parameters. The skinning weights \mathcal{W}_G and shape offsets $\Delta \mathbf{X}_{\text{shape}}$ are computed following [20, 40], allowing $W(\cdot)$ to transform the garment mesh via standard Linear Blend Skinning.

To recover physical realism, we employ a Physics-Informed GNN Φ_{GNN} to predict candidate deformations $\Delta \mathbf{X}_{\text{pred}}$. The network is conditioned on a physics-enriched graph \mathcal{G} encoding body proximity, force vectors, material parameters, and rest-state geometry:

$$\begin{aligned}\Delta \mathbf{X}_{\text{pred}} &= \Phi_{\text{GNN}}(\mathcal{G}(\mathbf{X}_{\text{coarse}}, \mathbf{V}_B)), \\ \mathbf{X}_{\text{pred}} &= \mathbf{X}_{\text{coarse}} + \Delta \mathbf{X}_{\text{pred}}.\end{aligned}\tag{2}$$

To ensure physical validity, we refine the prediction via a two-stage solver. We first eliminate residual forces using a learnable Force Solver $\mathcal{S}_{\text{force}}$, which iteratively resolves unbalanced forces from StVK deformation to reach equilibrium. This is followed by a differentiable projection $\mathcal{P}_{\text{proj}}$ to strictly enforce collision constraints against the body \mathbf{V}_B :

$$\begin{aligned}\mathbf{X}' &= \mathcal{S}_{\text{force}}(\mathbf{X}_{\text{pred}}), \\ \mathbf{X}^* &= \mathcal{P}_{\text{proj}}(\mathbf{X}'; \mathbf{V}_B).\end{aligned}\tag{3}$$

Crucially, the entire pipeline is fully differentiable, enabling end-to-end training via physical supervision.

3.2 Physical Energies and Forces

We employ StVK-based energy functions [39] to drive self-supervised training. Following DrapeNet [9], we model draping as a quasi-static process, omitting inertial terms to focus on equilibrium. The total objective \mathcal{L} aggregates strain, bending, collision, and gravitational potentials:

$$\mathcal{L} = E_{\text{strain}} + E_{\text{bend}} + E_{\text{coll}} + E_{\text{grav}}.\tag{4}$$

We formulate garment draping as a quasi-static process, assuming negligible inertial effects. Based on these potentials, we derive explicit residual force corresponding to each physical component. These forces constitute the fundamental driver of our pipeline: the internal forces define the minimization objective for the Force Solver to restore equilibrium, while the force state provides the GNN with physics-aware features to perceive both deformation and collision. Specifically, the explicit formulations for these forces are given by:

$$\begin{aligned}\mathbf{f}_{\text{strain}} &= \sum_{T \in \mathcal{N}(i)} -A_T h \mathbf{F}_T \left(\mu \mathbf{G}_T + \frac{\lambda}{2} \text{tr}(\mathbf{G}_T) \mathbf{I} \right) \mathbf{b}_{i,T}, \\ \mathbf{f}_{\text{bend}} &= \sum_{e \in \mathcal{H}(i)} s_{i,e} k_{\text{bend}} \frac{\|\mathbf{x}_e\|^3}{8A_e^2} \theta_e \mathbf{n}_{i,e}, \\ \mathbf{f}_{\text{coll}} &= 3k_{\text{coll}} (\text{ReLU}(\epsilon - d_i))^2 \mathbf{n}_{\text{body}}, \\ \mathbf{f}_{\text{grav}} &= m_i \mathbf{g}.\end{aligned}\tag{5}$$

Here, $\mathbf{f}_{\text{strain}}$ models in-plane membrane deformation using the Green-Lagrange strain tensor \mathbf{G}_T and Lamé constants λ, μ , integrated over the rest area A_T with thickness h . \mathbf{f}_{bend} penalizes mean curvature via dihedral angles θ_e at edges. \mathbf{f}_{coll} imposes a repulsive force when the vertex-to-body distance d_i falls below a safety margin ϵ , directed along the nearest body normal \mathbf{n}_{body} .

3.3 Physics-Informed Graph Neural Network

We formulate the draping inference as a residual learning problem on the coarse initialization $\mathbf{X}_{\text{coarse}}$. The network Φ_{GNN} predicts vertex-wise displacements to approximate the equilibrium, conditioned on a graph \mathcal{G} that explicitly encodes the physical state of garment. We design node features \mathbf{h}_i and edge features \mathbf{e}_{ij} as follows:

$$\begin{aligned}\mathbf{h}_i &= [\mathbf{n}_i, d_i, \mathbf{f}_i^{\text{net}}, \mathbf{m}_i] \in \mathbb{R}^{11}, \\ \mathbf{e}_{ij} &= [\mathbf{x}_{ij}, \|\mathbf{x}_{ij}\|, \mathbf{x}_{ij}^0, l_{ij}^0] \in \mathbb{R}^8.\end{aligned}\quad (6)$$

Node Features. \mathbf{h}_i integrates geometric and physical state information. Crucially, it includes the *net residual force* $\mathbf{f}_i^{\text{net}} = \mathbf{f}_{\text{strain}} + \mathbf{f}_{\text{bend}} + \mathbf{f}_{\text{coll}} + \mathbf{f}_{\text{grav}}$, computed explicitly via Eq. 5. This term provides the network with the direct gradient direction toward equilibrium. Additionally, d_i denotes the signed distance to the body surface, and $\mathbf{m}_i = [\mu, \lambda, k_{\text{bend}}, m_i]$ explicitly encodes the local material properties, comprising the Lamé coefficients μ, λ for membrane stiffness, the bending coefficient k_{bend} , and the nodal mass m_i .

Edge Features. For edges, we concatenate relative geometry in both the deformed space ($\mathbf{x}_{ij} = \mathbf{x}_i - \mathbf{x}_j$) and the rest configuration ($\mathbf{x}_{ij}^0, l_{ij}^0$). This duality enables the network to directly perceive local stretch and orientation changes relative to the rest state.

Architecture. We implement Φ_{GNN} using an Encode-Process-Decode architecture [34]. The raw features are projected into latent embeddings and iteratively updated via L message passing layers to propagate physical constraints:

$$\begin{aligned}\mathbf{e}_{ij}^{(l+1)} &= \mathbf{e}_{ij}^{(l)} + \text{MLP}_{\text{edge}} \left(\mathbf{e}_{ij}^{(l)}, \mathbf{h}_i^{(l)}, \mathbf{h}_j^{(l)} \right), \\ \mathbf{h}_i^{(l+1)} &= \mathbf{h}_i^{(l)} + \text{MLP}_{\text{node}} \left(\mathbf{h}_i^{(l)}, \sum_{j \in \mathcal{N}(i)} \mathbf{e}_{ij}^{(l+1)} \right).\end{aligned}\quad (7)$$

Finally, a decoder projects the evolved node embeddings $\mathbf{h}_i^{(L)}$ to the residual displacement $\Delta \mathbf{X}_{\text{pred}}$ defined in Eq. 2.

3.4 Learnable Force Solver

To further eliminate residual forces and recover rigorous physical equilibrium, we employ a differentiable Force Solver $\mathcal{S}_{\text{force}}$. Taking the network prediction \mathbf{X}_{pred} as initialization $\mathbf{X}^{(0)}$, the solver iteratively updates vertex positions driven by the explicit internal force field. Specifically, at each iteration t , we compute the combined internal deformation and gravitational forces, denoted as \mathbf{F}_{int} , and update the state along the force direction to eliminate these residuals:

$$\mathbf{X}^{(t+1)} = \mathbf{X}^{(t)} + \eta_t \cdot \mathbf{F}_{\text{int}}(\mathbf{X}^{(t)}), \quad \eta_t = \eta_0 \cdot \gamma^t, \quad (8)$$

where η_0 is the initial learnable compliance factor (inverse stiffness), and $\gamma \in (0, 1)$ is a learnable decay rate to stabilize the force solving process as the system approaches equilibrium. We explicitly exclude collision forces during this stage to resolve material deformation independently of contact constraints.

We design the solver as a learnable module that is tightly coupled with the network prediction, operating as a quasi-static refinement layer that reliably reduces residual forces while preserving the predicted configuration. By adapting the update magnitude and decay across iterations, the solver achieves stable and robust convergence from \mathbf{X}_{pred} toward physical equilibrium, enabling a flexible balance between refinement accuracy and computational efficiency.

3.5 Differentiable Collision Projection

To strictly enforce the non-penetration constraint, we employ a differentiable projection layer $\mathcal{P}_{\text{proj}}$. For each candidate vertex $\mathbf{x}_i \in \mathbf{X}'$, we identify its nearest neighbor \mathbf{p}_i on the body surface \mathbf{V}_B and the corresponding surface normal \mathbf{n}_i . The signed distance is computed as $d_i = (\mathbf{x}_i - \mathbf{p}_i) \cdot \mathbf{n}_i$.

A collision occurs if $d_i < \epsilon$. We resolve this by projecting the vertex outward along the body normal \mathbf{n}_i :

$$\mathbf{x}_i^* = \mathbf{x}_i + \delta \cdot \text{ReLU}(\epsilon - d_i) \cdot \mathbf{n}_i, \quad (9)$$

where $\epsilon = 2 \times 10^{-3}$ and $\delta = 1.01$ is an over-relaxation factor.

Differentiability Analysis. Strictly speaking, the nearest-neighbor search involves a discrete selection of the triangle index, which is non-differentiable. However, to enable end-to-end learning, we treat the correspondence pair $(\mathbf{p}_i, \mathbf{n}_i)$ as locally constant during the backward pass. Formally, let \mathcal{L} be the total objective function. The gradient with respect to the input vertex \mathbf{x}_i is derived via the chain rule:

$$\frac{\partial \mathcal{L}}{\partial \mathbf{x}_i} = \frac{\partial \mathcal{L}}{\partial \mathbf{x}_i^*} \cdot \frac{\partial \mathbf{x}_i^*}{\partial \mathbf{x}_i} \quad (10)$$

Since the indices are detached from the computation graph (i.e., $\frac{\partial \mathbf{p}_i}{\partial \mathbf{x}_i} = \mathbf{0}$ and $\frac{\partial \mathbf{n}_i}{\partial \mathbf{x}_i} = \mathbf{0}$), the Jacobian of the projection operator simplifies to:

$$\frac{\partial \mathbf{x}_i^*}{\partial \mathbf{x}_i} \approx \mathbf{I} - \delta \cdot \mathbb{I}(d_i < \epsilon) \cdot (\mathbf{n}_i \mathbf{n}_i^T), \quad (11)$$

where $\mathbb{I}(\cdot)$ is the indicator function for active collisions. This formulation effectively linearizes the collision manifold locally, ensuring stable gradient flow $\mathbf{g}_{in} = \mathbf{g}_{out}(\mathbf{I} - \delta \mathbf{n}_i \mathbf{n}_i^T)$ that removes velocity components strictly orthogonal to the surface.

In our implementation, we set $\epsilon = 2 \times 10^{-3}$ and $\delta = 1.01$. Unlike disconnected post-processing [38], our projection is embedded within the end-to-end learning pipeline. This integration ensures that collision-induced deformations translate into valid strain penalties, effectively compelling the upstream GNN and Force Solver to proactively learn collision-aware priors.

4 Experiments

We first introduce the datasets, evaluation metrics and implementation detail. We then present a comparison of quantitative and qualitative draping results with state-of-the-art methods. Subsequently, we provide an in-depth analysis of the proposed learnable solvers, focusing on their convergence behavior and physical compliance. Finally, we verify the necessity of each component through extensive ablation studies.

4.1 Implementation Details and Metrics

Implementation Details. We implement our framework using PyTorch [15] and leverage PyTorch3D [37] for efficient geometric operations and rendering. The networks are trained on a single NVIDIA A100 GPU for 150,000 iterations. We use the Adam optimizer [51] with a learning rate of 5×10^{-5} . Consistent with the self-supervised protocol of DrapeNet [9], we train solely on static garment meshes in the canonical T-pose. Note that while our method supports variable material properties (e.g., stiffness and density), we align these parameters with the fixed settings used in DrapeNet [9] during the quantitative comparison to ensure a fair evaluation. We perform end-to-end training with the learnable solver set to a total of $T = 3$ iterations. For evaluation, we increase this to $T = 15$ to demonstrate the consistent performance improvements achieved with additional solver steps.

Network Architecture. The GNN is instantiated as an Encode-Process-Decode architecture [34]. The encoder maps input features to a 128-dimensional latent space. The processor consists of 16 message-passing blocks, where each block utilizes a 2-layer MLP with ReLU activation and Layer Normalization. The graph connectivity is defined by the garment’s mesh topology, augmented with bi-directional edges.

Datasets. We follow the experimental protocol established in DrapeNet [9] to utilize the CLOTH3D dataset [2] for both training and evaluation. However, we focus exclusively on upper-body garments. We randomly select 600 top garments (including t-shirts, shirts, and tank tops) from the dataset. Consistent with [9], we do not rely on the ground-truth simulated deformations provided by CLOTH3D for supervision; instead, we only utilize the garment template meshes in their canonical state (T-pose on an average body shape). For evaluation, we

employ a separate set of 30 top garments that are unseen during training. To ensure robustness across diverse body configurations, we sample body poses from the AMASS dataset [27] and sample body shape parameters β uniformly from the range $[-3, 3]^{10}$ during training.

Evaluation Metrics. Evaluating unsupervised garment draping is challenging due to the stochastic nature of cloth dynamics; multiple draped states can be physically valid for a single pose. Therefore, relying solely on Euclidean distance is often insufficient [9, 39]. Instead, we focus on physical energy and collision handling for quantitative evaluation, as they directly measure the physical plausibility and geometric validity of the draped garments. Following DrapeNet [9], we report three physics-based energy metrics: strain (E_{strain}) quantifying surface stretching, bending (E_{bend}) reflecting folding smoothness, and gravitational potential energy (E_{grav}). Lower energy values generally indicate a more relaxed and physically plausible state. Additionally, we report the Body-to-Garment (B2G) ratio to assess collision handling, calculated as the ratio of the surface area of garment faces penetrating the body to the total garment area.

4.2 Comparisons with State-of-the-Arts

Table 1: Quantitative comparison on unseen garments. We report physical energy metrics (E_{strain} , E_{bend} , E_{grav}) and interpenetration ratios (B2G) on the CLOTH3D test set. PhysDrape achieves the best performance across all metrics, significantly reducing strain and B2G.

Method	$E_{\text{strain}} \downarrow$	$E_{\text{bend}} \downarrow$	$E_{\text{grav}} \downarrow$	B2G % \downarrow
DeePSD [4]	7.22	0.01	0.98	7.2
DIG [20]	6.32	0.01	1.05	1.8
DrapeNet [9]	0.43	0.01	1.05	0.9
PhysDrape ($T = 3$)	0.20	0.004	1.01	0.05
PhysDrape ($T = 15$)	0.15	0.004	1.01	0.05

Quantitative Comparison. We compare PhysDrape with three state-of-the-art approaches: DeePSD [4], DIG [20], and DrapeNet [9]. We exclude dynamic simulators (e.g., SNUG [39], GAPS [7]) from quantitative comparison, as they model inertial effects and time integration, which are fundamentally different from the history-free equilibrium problem addressed in this work. Moreover, unlike PhysDrape, these methods are often confined to specific garment templates, making fair comparison on unseen topologies infeasible. To ensure a fair comparison, all methods are evaluated on the same unseen test set from CLOTH3D. As reported in Table 1, the baseline methods, DeePSD and DIG, exhibit high strain energies (> 6.0) and noticeable B2G ratios (7.2% and 1.8%, respectively),

as they lack collision handling mechanisms. While DrapeNet improves physical plausibility via self-supervision, it still retains a B2G ratio of 0.9%. In contrast, PhysDrape ($T = 15$) significantly outperforms these baselines. By integrating the explicit solver, our method reduces the strain energy to 0.15 while minimizing collisions to a negligible level ($B2G \approx 0.05\%$). This indicates that our approach achieves a more physically consistent equilibrium with superior geometric validity.

Qualitative Comparison. We visually compare the draping quality against DrapeNet in Fig. 3. As highlighted by the red boxes, the baseline method suffers from severe artifacts, exhibiting explicit interpenetrations in complex contact regions such as the armpits, shoulders, and back. These artifacts indicate a failure to resolve collisions in challenging high-curvature or high stress areas. These failures typically occur in high-curvature areas where soft penalties are insufficient to resolve constraints. In contrast, PhysDrape generates smooth, continuous, and collision-free garments that tightly conform to the body shape, validating the effectiveness of our hard-constrained projection in handling complex body-garment interactions.

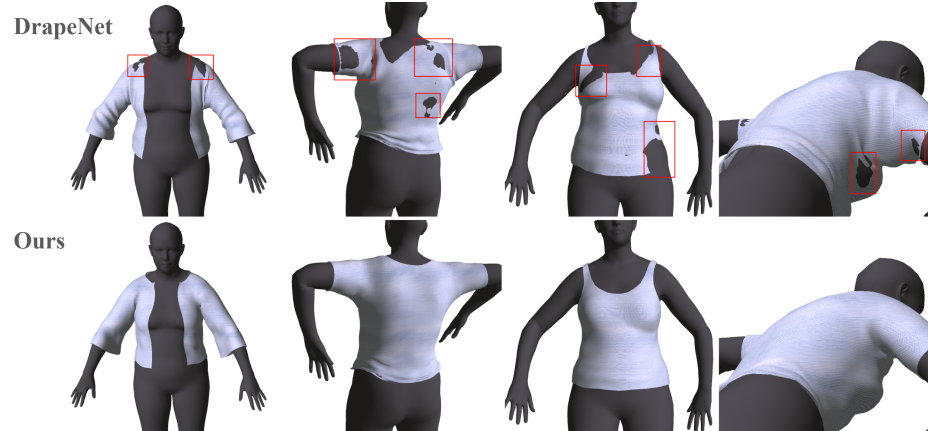


Fig. 3: Visual comparison of collision handling on unseen body poses. The baseline method (top row) fails to resolve complex contacts, resulting in visible interpenetrations in complex regions such as the armpits and shoulders (highlighted in red). In contrast, PhysDrape (bottom row) strictly enforces geometric constraints, generating smooth and collision-free garments that robustly adapt to the body shape.

4.3 Learnable Solver and Physical Controllability

We analyze the effectiveness of our differentiable solver through iteration dynamics and material generalization.

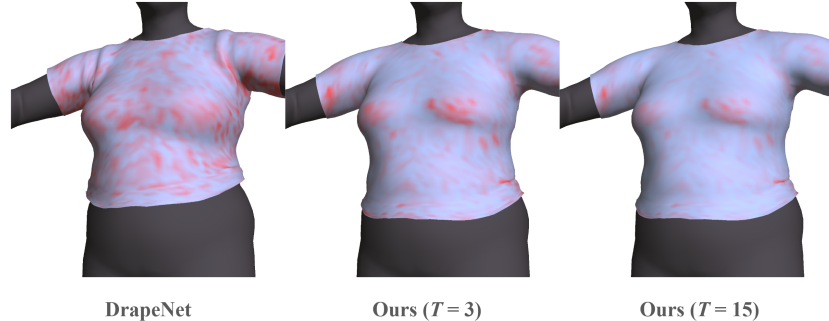


Fig. 4: Visualization of physical relaxation and force dissipation. We map residual forces to a heatmap where red denotes high stress. While DrapeNet exhibits widespread unnatural stretching, our solver effectively dissipates these forces from $T = 3$ to $T = 15$, reaching a stable and physically consistent equilibrium.

Impact of Solver Iterations. To validate the role of our two-stage coupling, we evaluate the performance at early ($T = 3$) and converged ($T = 15$) solver steps in Table 1. As shown in the B2G metric, our method achieves a near-zero B2G ratio of 0.05% even at $T = 3$, confirming that the projection layer efficiently handles most of the penetration immediately. Extending iterations to $T = 15$ further reduces the strain energy (E_{strain} drops from 0.20 to 0.15). We visualize this physical relaxation process in Fig. 4. At the early stage ($T = 3$), we observe residual forces in high-stress regions (shown in red). As the solver iterates to $T = 15$, these forces are effectively dissipated (turning blue), indicating that the mesh has relaxed to a stable equilibrium. This convergence behavior is quantitatively analyzed in Fig. 5, where both the total energy and residual forces drop significantly and stabilize, demonstrating that our solver reliably guides the mesh toward a lower-energy state.

Robustness to Material Properties. Furthermore, we demonstrate the physical controllability of our method in Fig. 6. By adjusting the stiffness parameters in both the network input and the differentiable solver, PhysDrape generates distinct draping behaviors—ranging from ‘Soft’ materials with rich folds to ‘Hard’ materials with structural rigidity and smoother surfaces—without requiring network retraining.

4.4 Ablation Studies

We conduct ablation studies to validate our design choices, specifically analyzing the contribution of individual modules and the impact of solver iterations.

Impact of Explicit Constraints. To validate the necessity of each component, we evaluate two variants in Table 2: removing the learnable force solver (w/o Solver) and removing the differentiable projection (w/o Projection). As

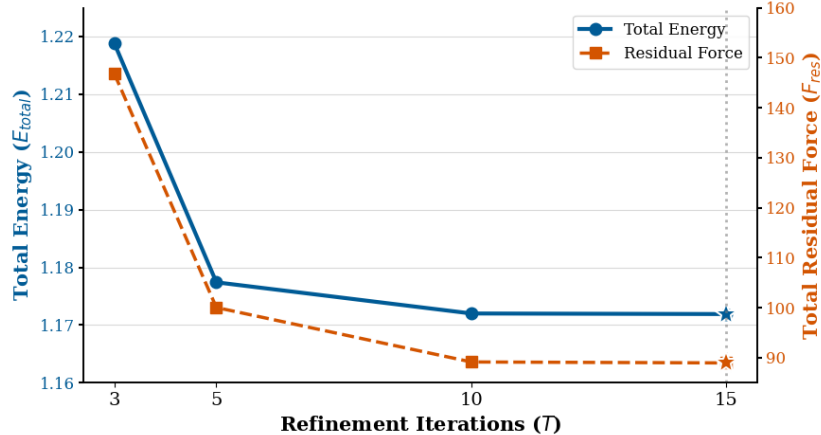


Fig. 5: Convergence analysis of the learnable solver. We plot Total Energy (E_{total} , blue) and Residual Force (F_{res} , orange) over iterations T . The sharp decrease and subsequent stabilization demonstrate that our solver efficiently drives the mesh to a physically consistent equilibrium.

shown in the first row, relying solely on projection forces the mesh into valid geometric positions but fails to resolve internal stress, resulting in higher strain energy ($E_{strain} \approx 0.23$) and stiff deformations. Conversely, ablating the projection layer (w/o Projection) allows the solver to minimize strain energy effectively (0.15) but fails to guarantee geometric validity, leading to a significant B2G ratio (2.29%). Our full model couples both modules to achieve the optimal balance: it effectively relaxes internal forces via the solver while the projection layer strictly enforces constraints ($B2G \approx 0.05\%$), ensuring robust and physically plausible draping.

Table 2: Ablation study on explicit constraints. We evaluate the impact of the learnable force solver and the projection layer. The Full Model achieves the optimal balance, minimizing strain energy while strictly enforcing collision constraints.

Method	$E_{strain} \downarrow$	B2G % \downarrow
w/o Solver	0.23	0.05
w/o Projection	0.15	2.29
Full Model	0.15	0.05

Runtime Impact of Solver Iterations. We measure the inference speed on a single NVIDIA V100 GPU. The time per frame increases from 30 ms at $T = 3$, 45 ms at $T = 5$, 70 ms at $T = 10$ and 90 ms at $T = 15$. Real-time performance is achieved at low iteration counts, while higher iterations remain interactive, allowing a flexible trade-off where increased iterations further reduce strain energy for improved physical fidelity.

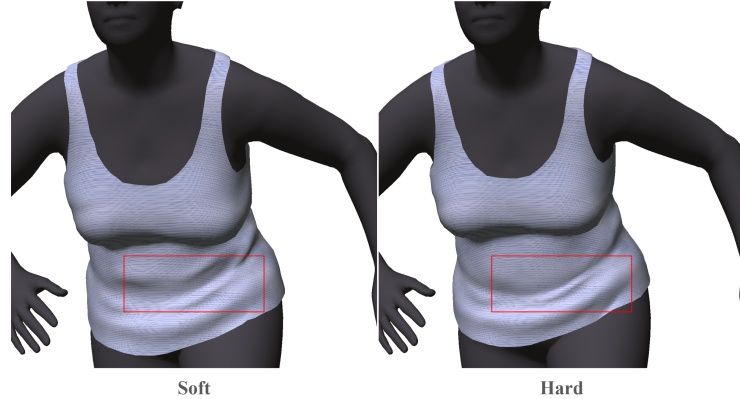


Fig. 6: Physical controllability via material stiffness. By modulating the material parameters in both the network input condition and the StVK solver, our method generates distinct draping behaviors using the same trained model. The Soft material (left) exhibits rich, high-frequency folds, while the Hard material (right) maintains a stiffer silhouette with smoother deformations (highlighted in the red box).

5 Conclusion

In this paper, we presented PhysDrape, a hybrid neural-physical framework that achieves physically realistic garment draping. Unlike existing methods that rely on soft penalties, which force a trade-off between geometric feasibility and physical plausibility, PhysDrape integrates a Physics-Informed GNN with a differentiable explicit solver. By coupling a learnable Force Solver based on the StVK model with a Differentiable Projection Layer, our pipeline reduces the interpenetration ratio to a negligible level ($B2G \approx 0.05\%$) while minimizing residual forces to ensure physical fidelity. Extensive experiments demonstrate that PhysDrape achieves state-of-the-art performance, generating negligible interpenetration garments with significantly lower strain energy compared to baselines, all while maintaining real-time inference speeds.

Limitations and Future Work. PhysDrape resolves collisions in real-time but currently neglects inertial effects due to its quasi-static formulation. Future work will extend the solver to full animation and leverage differentiability for inverse garment reconstruction [9]. Additionally, integrating implicit representations or sewing pattern optimization [21, 23] shows promise for handling complex multi-layered garments.

Acknowledgements

We thank Zirui Tang (Yangtze Normal University) for meaningful insights and her assistance in rendering and the visualization of results.

References

1. Baraff, D., Witkin, A.: Large steps in cloth simulation. In: Seminal Graphics Papers: Pushing the Boundaries, Volume 2, pp. 767–778 (2023)
2. Bertiche, H., Madadi, M., Escalera, S.: Cloth3d: clothed 3d humans. In: European Conference on Computer Vision. pp. 344–359. Springer (2020)
3. Bertiche, H., Madadi, M., Escalera, S.: Pbns: physically based neural simulator for unsupervised garment pose space deformation. arXiv preprint arXiv:2012.11310 (2020)
4. Bertiche, H., Madadi, M., Tylson, E., Escalera, S.: Deepsd: Automatic deep skinning and pose space deformation for 3d garment animation. In: Proceedings of the IEEE/CVF international conference on computer vision. pp. 5471–5480 (2021)
5. Bhatnagar, B.L., Tiwari, G., Theobalt, C., Pons-Moll, G.: Multi-garment net: Learning to dress 3d people from images. In: Proceedings of the IEEE/CVF international conference on computer vision. pp. 5420–5430 (2019)
6. Bouaziz, S., Martin, S., Liu, T., Kavan, L., Pauly, M.: Projective dynamics: Fusing constraint projections for fast simulation. In: Seminal Graphics Papers: Pushing the Boundaries, Volume 2, pp. 787–797 (2023)
7. Chen, R., Chen, L., Parashar, S.: Gaps: Geometry-aware, physics-based, self-supervised neural garment draping. In: 2024 International Conference on 3D Vision (3DV). pp. 116–125. IEEE (2024)
8. Chibane, J., Pons-Moll, G., et al.: Neural unsigned distance fields for implicit function learning. Advances in Neural Information Processing Systems **33**, 21638–21652 (2020)
9. De Luigi, L., Li, R., Guillard, B., Salzmann, M., Fua, P.: Drapenet: Garment generation and self-supervised draping. In: Proceedings of the IEEE/CVF conference on computer vision and pattern recognition. pp. 1451–1460 (2023)
10. Designer, M.: <https://www.marvelousdesigner.com/> (2026)
11. Etzmuss, O., Gross, J., Strasser, W.: Deriving a particle system from continuum mechanics for the animation of deformable objects. IEEE Transactions on Visualization and Computer Graphics **9**(4), 538–550 (2003)
12. Grigorev, A., Black, M.J., Hilliges, O.: Hood: Hierarchical graphs for generalized modelling of clothing dynamics. In: Proceedings of the IEEE/CVF conference on computer vision and pattern recognition. pp. 16965–16974 (2023)
13. Gundogdu, E., Constantin, V., Parashar, S., Seifoddini, A., Dang, M., Salzmann, M., Fua, P.: Garnet++: Improving fast and accurate static 3d cloth draping by curvature loss. IEEE Transactions on Pattern Analysis and Machine Intelligence **44**(1), 181–195 (2020)
14. Gundogdu, E., Constantin, V., Seifoddini, A., Dang, M., Salzmann, M., Fua, P.: Garnet: A two-stream network for fast and accurate 3d cloth draping. In: Proceedings of the IEEE/CVF international conference on computer vision. pp. 8739–8748 (2019)
15. Imambi, S., Prakash, K.B., Kanagachidambaresan, G.: Pytorch. In: Programming with TensorFlow: solution for edge computing applications, pp. 87–104. Springer (2021)
16. Islam, T., Miron, A., Liu, X., Li, Y.: Deep learning in virtual try-on: A comprehensive survey. IEEE Access **12**, 29475–29502 (2024)
17. Lewiner, T., Lopes, H., Vieira, A.W., Tavares, G.: Efficient implementation of marching cubes' cases with topological guarantees. Journal of graphics tools **8**(2), 1–15 (2003)

18. Li, M., Ferguson, Z., Schneider, T., Langlois, T.R., Zorin, D., Panozzo, D., Jiang, C., Kaufman, D.M.: Incremental potential contact: intersection-and inversion-free, large-deformation dynamics. *ACM Trans. Graph.* **39**(4), 49 (2020)
19. Li, R., Guillard, B., Fua, P.: Isp: Multi-layered garment draping with implicit sewing patterns. *Advances in Neural Information Processing Systems* **36**, 40294–40319 (2023)
20. Li, R., Guillard, B., Remelli, E., Fua, P.: Dig: Draping implicit garment over the human body. In: *Proceedings of the Asian conference on computer vision*. pp. 2780–2795 (2022)
21. Li, X., Yu, C., Du, W., Jiang, Y., Xie, T., Chen, Y., Yang, Y., Jiang, C.: Dress-1-to-3: Single image to simulation-ready 3d outfit with diffusion prior and differentiable physics. *ACM Transactions on Graphics (TOG)* **44**(4), 1–16 (2025)
22. Liao, Z., Wang, S., Komura, T.: Senc: Handling self-collision in neural cloth simulation. In: *European Conference on Computer Vision*. pp. 385–402. Springer (2024)
23. Liu, L., Xu, X., Lin, Z., Liang, J., Yan, S.: Towards garment sewing pattern reconstruction from a single image. *ACM Transactions on Graphics (TOG)* **42**(6), 1–15 (2023)
24. Liu, T., Bouaziz, S., Kavan, L.: Quasi-newton methods for real-time simulation of hyperelastic materials. *Acm Transactions on Graphics (TOG)* **36**(3), 1–16 (2017)
25. Loper, M., Mahmood, N., Romero, J., Pons-Moll, G., Black, M.J.: Smpl: A skinned multi-person linear model. In: *Seminal Graphics Papers: Pushing the Boundaries*, Volume 2, pp. 851–866 (2023)
26. Macklin, M., Müller, M., Chentanez, N.: Xpbd: position-based simulation of compliant constrained dynamics. In: *Proceedings of the 9th International Conference on Motion in Games*. pp. 49–54 (2016)
27. Mahmood, N., Ghorbani, N., Troje, N.F., Pons-Moll, G., Black, M.J.: Amass: Archive of motion capture as surface shapes. In: *Proceedings of the IEEE/CVF international conference on computer vision*. pp. 5442–5451 (2019)
28. Müller, M., Heidelberger, B., Hennix, M., Ratcliff, J.: Position based dynamics. *Journal of Visual Communication and Image Representation* **18**(2), 109–118 (2007)
29. Nvidia: Nvcloth (2018)
30. Nvidia: Nvidia flex. <https://developer.nvidia.com/flex> (2018)
31. Optitex: Optitex fashion design software. <https://optitex.com/> (2018)
32. Park, J.J., Florence, P., Straub, J., Newcombe, R., Lovegrove, S.: Deepsdf: Learning continuous signed distance functions for shape representation. In: *Proceedings of the IEEE/CVF conference on computer vision and pattern recognition*. pp. 165–174 (2019)
33. Patel, C., Liao, Z., Pons-Moll, G.: Tailornet: Predicting clothing in 3d as a function of human pose, shape and garment style. In: *Proceedings of the IEEE/CVF conference on computer vision and pattern recognition*. pp. 7365–7375 (2020)
34. Pfaff, T., Fortunato, M., Sanchez-Gonzalez, A., Battaglia, P.: Learning mesh-based simulation with graph networks. In: *International conference on learning representations* (2020)
35. Provot, X.: Collision and self-collision handling in cloth model dedicated to design garments. In: *Computer Animation and Simulation'97: Proceedings of the Eurographics Workshop in Budapest, Hungary, September 2–3, 1997*. pp. 177–189. Springer (1997)
36. Provot, X., et al.: Deformation constraints in a mass-spring model to describe rigid cloth behaviour. In: *Graphics interface*. pp. 147–147. Canadian Information Processing Society (1995)

37. Ravi, N., Reizenstein, J., Novotny, D., Gordon, T., Lo, W.Y., Johnson, J., Gkioxari, G.: Accelerating 3d deep learning with pytorch3d. arXiv preprint arXiv:2007.08501 (2020)
38. Santesteban, I., Otaduy, M.A., Casas, D.: Learning-based animation of clothing for virtual try-on. In: Computer Graphics Forum. vol. 38, pp. 355–366. Wiley Online Library (2019)
39. Santesteban, I., Otaduy, M.A., Casas, D.: Snug: Self-supervised neural dynamic garments. In: Proceedings of the IEEE/CVF conference on computer vision and pattern recognition. pp. 8140–8150 (2022)
40. Santesteban, I., Thuerey, N., Otaduy, M.A., Casas, D.: Self-supervised collision handling via generative 3d garment models for virtual try-on. In: Proceedings of the IEEE/CVF Conference on Computer Vision and Pattern Recognition. pp. 11763–11773 (2021)
41. Shi, W., Wong, W., Zou, X.: Generative ai in fashion: Overview. ACM Transactions on Intelligent Systems and Technology **16**(4), 1–73 (2025)
42. Stuyck, T., Chen, H.y.: Diffxpbd: Differentiable position-based simulation of compliant constraint dynamics. Proceedings of the ACM on Computer Graphics and Interactive Techniques **6**(3), 1–14 (2023)
43. Su, T., Zhang, Y., Zhou, Y., Yu, Y., Du, S.: Gpu-based real-time cloth simulation for virtual try-on. In: PG (Short Papers and Posters). pp. 1–2 (2018)
44. Tan, Q., Zhou, Y., Wang, T., Ceylan, D., Sun, X., Manocha, D.: A repulsive force unit for garment collision handling in neural networks. In: European conference on computer vision. pp. 451–467. Springer (2022)
45. Tang, M., Yuan, R., Kou, D., Sun, M., Zhang, L.: Saf: Local shape-aware face-based garment collision handling via neural sdf. In: ICASSP 2025-2025 IEEE International Conference on Acoustics, Speech and Signal Processing (ICASSP). pp. 1–5. IEEE (2025)
46. Tiwari, L., Bhowmick, B., Sinha, S.: Gensim: Unsupervised generic garment simulator. In: Proceedings of the IEEE/CVF Conference on Computer Vision and Pattern Recognition. pp. 4169–4178 (2023)
47. Vassilev, T., Spanlang, B., Chrysanthou, Y.: Fast cloth animation on walking avatars. In: Computer Graphics Forum. vol. 20, pp. 260–267. Wiley Online Library (2001)
48. Venkatesh, R., Karmali, T., Sharma, S., Ghosh, A., Babu, R.V., Jeni, L.A., Singh, M.: Deep implicit surface point prediction networks. In: Proceedings of the IEEE/CVF international conference on computer vision. pp. 12653–12662 (2021)
49. Xi, N., Hamari, J.: Shopping in virtual reality: A literature review and future agenda. Journal of Business Research **134**, 37–58 (2021)
50. Zeller, C.: Cloth simulation on the gpu. In: ACM SIGGRAPH 2005 Sketches, pp. 39–es (2005)
51. Zhang, Z.: Improved adam optimizer for deep neural networks. In: 2018 IEEE/ACM 26th international symposium on quality of service (IWQoS). pp. 1–2. Ieee (2018)
52. Zhao, F., Wang, W., Liao, S., Shao, L.: Learning anchored unsigned distance functions with gradient direction alignment for single-view garment reconstruction. In: Proceedings of the IEEE/CVF International Conference on Computer Vision. pp. 12674–12683 (2021)